Journal Pre-proof

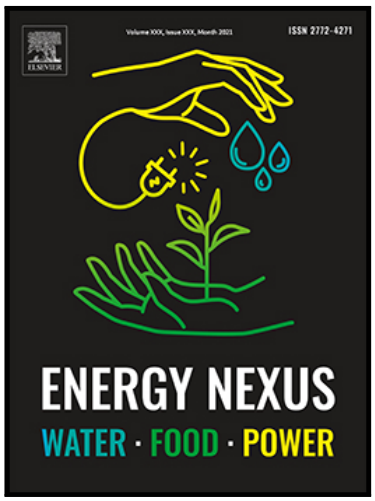

Modeling Current and Future Run-off and Soil Erosion Dynamics in Eastern Mediterranean Ecosystems Using the WEPP Model

Safwan Mohammed

PII: S2772-4271(25)00016-6
DOI: https://doi.org/10.1016/j.nexus.2025.100375
Reference: NEXUS 100375

To appear in: *Energy Nexus*

Received date: 3 September 2024
Revised date: 22 January 2025
Accepted date: 8 February 2025

Please cite this article as: Safwan Mohammed , Modeling Current and Future Run-off and Soil Erosion Dynamics in Eastern Mediterranean Ecosystems Using the WEPP Model, *Energy Nexus* (2025), doi: https://doi.org/10.1016/j.nexus.2025.100375

Highlights

- Soil erosion (SE) and runoff (RF) were analyzed in three eastern Mediterranean ecosystems.
- The Water Erosion Prediction Project (WEPP) model was used to predict SE and RF.
- The WEPP model was efficient in predicting SE and RF.
- Agricultural land was more susceptible to projected SE and RF.
- The WEPP model predicted the peaks for SE and RF would be in 2025 and 2035.

Modeling Current and Future Run-off and Soil Erosion Dynamics in Eastern Mediterranean Ecosystems Using the WEPP Model

Safwan Mohammed [1,2*]

[1] Institutes for Agricultural Research and Educational Farm, University of Debrecen, Böszörményi 138, H-4032 Debrecen, Hungary.
[2] Earth Science Institute, Slovak Academy of Sciences, Dúbravská cesta 9, 840 05 Bratislava, Slovak Republic.
[*]Correspondence: safwan@agr.unideb.hu

Abstract:

Run-off (RF) and soil erosion (SE) have a negative impact on the environmental system, with both on-site and off-site effects. This research aimed to evaluate the performance of the Water Erosion Prediction Project (WEPP) model in predicting SE and RF across four locations representing three ecosystems: agricultural land (location-KS at 8% slope, location-MN at 20% slope), forest (location-AINF at 35% slope), and burned forest (location-AINBF at 35% slope). It also predicts the future responses of the studied ecosystems to SE and RF for the upcoming 20 years. The study was conducted in the eastern Mediterranean from 2019 to 2038, 2019 served as the reference year to compare WEPP model output with measured values at the studied locations. Model performance indicators showed the applicability of WEPP model in predicting SE (model efficiency (NSE) =0.67, coefficient of determination (R^2) =0.97), RF (NSE=0.66, R^2=0.78). Future projections revealed that the agricultural ecosystem exceeded others in terms of SE and RF. However, annual RF can be ranked as follows: KS (234.7mm±75.6)> MN (141.1mm±50.2)> AINF (145.4mm±47.4) > AINBF (100.3mm±49.2). Similarly, SE can be classified as: KS (2.38 kg/m^2 ±1.36)> AINF (0.45 kg/m^2 ±0.17) > MN (0.31 kg/m^2 ±0.11)> AINBF (0.24 kg/m^2 ±0.15). However, monthly results of SE and RF were more intense in the KS location and less pronounced in the rest of the ecosystems. An analysis of associated factors, namely, soil water content (θ, %), and soil water hydraulic conductivity (K_{sw}, mm/hr), revealed the lowest θ values occurred during the summer season (June to August), reaching 46.3%, 50.3%, 46.2%, and 49.2%, for KS, MN, AINF, and AINBF, respectively. Conversely, the highest K_{sw} was forecasted in summer, ranging from 3.3 to 6.3 mm/hr. This research promotes utilizing the WEEP model as a sustainable tool for ecosystem management in the eastern Mediterranean, aiding decision-makers in rehabilitation planning.

Keywords: Erosion; Modeling; Soil Conservation; Rainfall Erosivity; Syria.

Graphical Abstract:

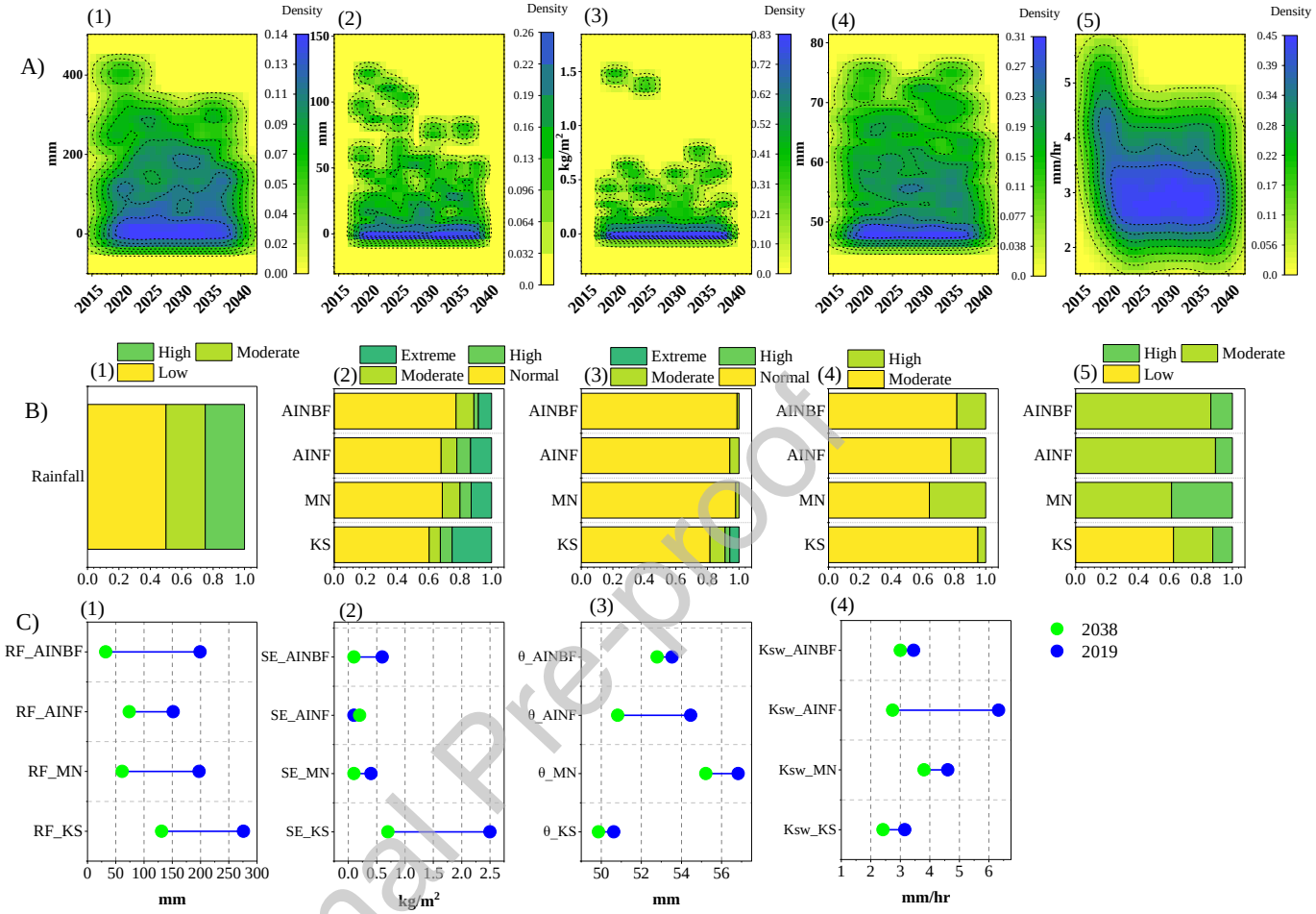

Highlights

- Soil erosion (SE) and run-off (RF) were analyzed in three eastern Mediterranean ecosystems.
- The Water Erosion Prediction Project (WEPP) model was used to predict SE and RF.
- The WEPP model was efficient in predicting SE and RF.
- Agricultural land was more susceptible to projected SE and RF.
- The WEPP model predicted the peaks for SE and RF would be in 2025 and 2035.

1. Introduction

Land degradation is one of the major threats to the sustainability of the environmental system and ecosystem services worldwide. Land degradation includes pollution, desertification, salinization, fertility reduction, and soil erosion. Recently, van Leeuwen et al. (2019) reported that the activities of at least 3.2 billion people are suffering from the negative consequences of it. Hence, more efforts should be made to mitigate land degradation and support the achievement of Sustainable Development Goals (UN-SDGs) (Griggs et al., 2013, Keesstra et al. 2016)., especially in the era of climate change.

Soil erosion is one of the threats to ecosystem balance and improvement, referring to the process of movement of soil particles from one point to another, usually from the basin or watershed to the outlet/waterbody. Soil erosion has a negative impact on the environmental system, with both on-site and off-site effects. On-site effects include deterioration of soil physical and chemical properties as a direct result of destruction of soil structure and leaching of nutrients (Kulimushi et al., 2021a, b). Soil erosion is also linked to further reduction in available soil moisture and can accelerated by drought conditions (Tenge et al. 1998). The net result is a loss of productivity that limits what can be grown and involves increased fertilizer consumption to maintain yields (Bakker et al. 2004). Off-site problems result from downstream or downwind sedimentation that pollutes natural waterbodies (lakes, reservoirs), clogs irrigation canals and reduces the design life of reservoirs (Duan et al., 2011; Poesen, 2018). Sediment is a contaminant which can increase nitrogen and phosphorus levels in waterbodies, leading to eutrophication (Borrelli et al., 2017; Varvani et al., 2019).

Several methods have been used to measure and evaluate soil erosion, ranging from experimental measurements at specific locations to modeling approaches on a watershed scale. Experimental measurement of soil erosion involves the installation of plots of different lengths, which can be categorized into various methods, namely levelling, volumetric, deluometric, deflametric, climatological, pluviological, and monolithic (Zachar 1982). A significant advantage of this approach is the ability to obtain accurate measurements of soil erosion and Run-off. However, it is time-consuming, requires considerable investment in terms of budget, and demands substantial labor work.

Due to limitations of the experimental methods, many models have been developed to simulate the soil erosion process. In this sense, models for assessing soil erosion can be divided into three

groups: empirical models, with the well-known Universal Soil Loss Equation (RUSLE) (Renard, 1997). As an example, physical models, exemplified by the Water Erosion Prediction Project model (WEPP) (Nearing, 1998); and hybrid/conceptual models, such as the Large-Scale Catchment Model. All these models simplify the erosion process and provide useful tools for predicting soil erosion. However, these models require a large amount of data, which is sometimes not available, and their outputs are subject to overprediction or underestimation. Recently, machine learning and big data have started to be utilized for predicting soil erosion, offering a new tool for assessment and evaluation (Sahour et al. 2021).

In the Mediterranean basin, soil erosion poses significant challenges to the sustainability of natural resources (García-Ruiz, 2010). Hence, topographical aspects, shallow soil, massive change in land use towards agricultural land, along with heavy rainstorms, accelerate the erosion process and threaten the Mediterranean ecosystem balance. Several investigations were conducted in the m Mediterranean basin to illustrate the impact of soil water erosion and even wind erosion on the ecosystem and sustainability of natural resources. For instance, in Southern Spain (Gómez et al., 2014), South Italy, (Pampalone et al. 2022), Portugal (Nunes et al., 2023), Lebanon (Kheir et al. 2006), and Morrocco (d'Oleire-Oltmanns et al. 2012). In this context, various methods were adopted, such as observed plots (Comino et al. 2016), the USLE/RUSLE (Abdo, 2018), machine learning algorithms (Barakat et al., 2023), Unmanned Aerial Vehicle (UAV) (d'Oleire-Oltmanns et al. 2012), SWAT, and AnnAGNPS (Abdelwahab et al. 2018). The WEPP model as one of the adopted models in the Mediterranean region has shown varied outcomes. In Spain, Soto & Díaz-Fierros (1998) reported that the WEPP performance was acceptable. Conversely, in Tunisia, Raclot & Albergel (2006) noted an unsatisfactory performance of the WEPP model due to improper simulation of some soil characteristics, such as cracking. In Iran, the model was satisfactory performing with r=0.61, however underestimation was recorded (Mahmoodabadi & Cerdà 2013). Overall, **Figure 1** illustrates the dynamic correlation between the WEPP model, Run-off, and soil erosion based on published research in Scopus database.

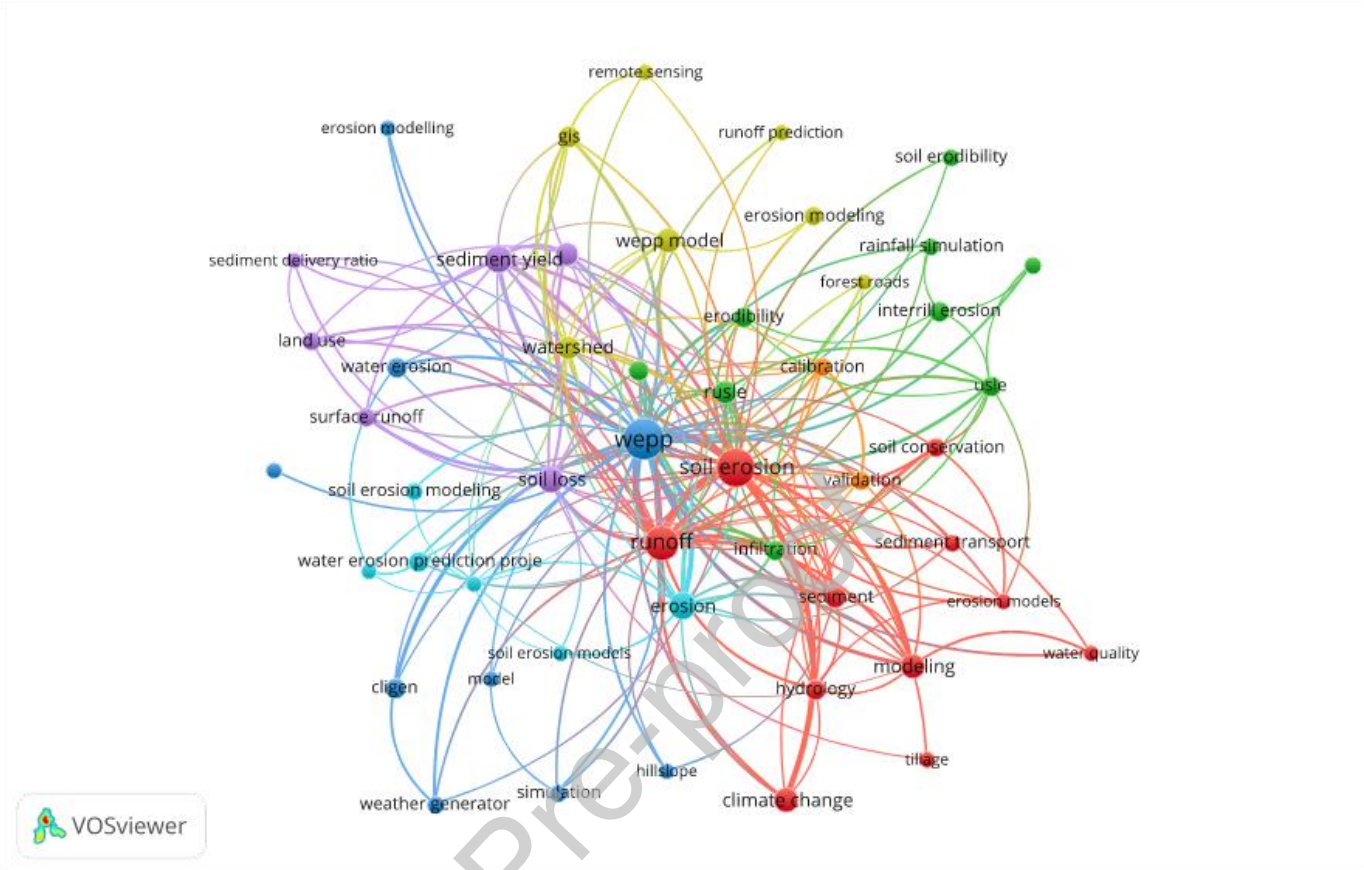

Fig.1: Bibliometric analysis of the keywords appears on research database of WOS based on the following equations ("soil erosion" OR "soil loss" OR "land degradation") AND ("Run-off" OR "surface Run-off" OR "water erosion") AND WEPP). (N=415)

In Syria, soil erosion is one of the natural hazards threatening the ecosystem and sustainability of the agricultural sector. Hence, climate change, extreme rainfall events, agricultural activities, forest fires, and deforestation contribute to the acceleration of soil erosion and run-off (Abdo, 2018; Mohammed et al., 2020; Abdo, 2022). However, both experimental methods and modeling approaches have been used to assess erosion and its factors in Syria. For instance, experimental monitoring plots in West Syria indicate that inclination and agricultural activities have a devastating impact on the topsoil layer and accelerate erosion, where the erosion ranged between 0.368 kg/m^2 to 1.145 kg/m^2 (Mohammed et al., 2021a). On the other hand, Mohammed et al. (2020) used RUSLE-GIS to predict soil erosion in the southern part of Syria, which ranged from 1.26 to 350.5 t/ha/year. The same method was adopted by Abdo, & Salloum, (2017) in the west of

Syria and reported that ranges from 0 to 22.3 t/ha/year. Interestingly, Richi (2025) recommended using RUSLE-GIS to support local environmental planners in the coastal region of Syria.
In this context, a very limited number of studies have used the WEPP model to predict soil erosion in Syria, where a good fit between WEPP and RUSLE was reported (Mohammed et al., 2021b). However, modeling soil erosion using the WEPP model provides an opportunity to predict the amount of eroded soil and run-off in the coastal region of Syria. This approach can aid in preparing rehabilitation plans for the coastal region and contribute to the recovery stage of the country. Hence, more in-depth research related to the applicability of the WEPP model for predicting soil erosion and run-off is needed for sustainable planning post-war. The detailed goals are to evaluate the performance of the WEPP model in predicting soil erosion and run-off in four different locations representing three types of ecosystems: agricultural land, forest, burned forest, and to predict future erosion and run-off under predicted climate models.

2. Material and method

2.1. Study area and data collection

This study was conducted in the eastern Mediterranean, specifically in A-Sahel basin of western Syria. The average temperature ranges between 16-25°C, and the average rainfall of approximately 750 mm annually (Mohammed et al. 2021a). However, the study area exhibits a Mediterranean climate which is characterized by rainy winters and dry summers. Most of the soil is classified as Entisols (Mohammed et al. 2020), where agriculture is one of the major activities for the local residents. In the eastern Mediterranean, the predominant land use/land cover groups include forest, agricultural land, and urban area.

Based on the literature, four different locations were chosen to predict current and future soil erosion and Run-off. The selection of locations was primarily based on varying land use and slope, representing the study area comprehensively. **Table 1** provides a full overview of the chosen locations and their characteristics.

Table 1 Characterization of the three ecosystems and four studied locations

Location	Ecosystem	Slope	Depth	Silt	Clay	Sand	Texture	OM	CEC	θ_i	Rock	K_{ec}	SE	RF	Reference
		%	mm	%	%	%		%		%	%	mm/h	kg/m^2	mm	

KS[1]	Agriculture	8	254	24.01	38.12	37.87	L	1.3	33	25	10	-	4.4	280	Mohammed et al. (2023)
MN[2]		20	245	14	56	30	CL	3.9	24	24	8	10	0.96	138	Mohammed et al. (2021)
AINF	Forest	35	15	20	50	30	CL	5.3	23	25	8	7	0.01	155	Al-Ali et al. (2014)
AINFR	Burned forest	35	15	20	50	30	CL	2.3	22	25		7	0.72	175	

1: pomegranate, 2: winter wheat, θ_i%: initial saturation level, K_{ec}: effective hydraulic conductivity

2.2. Modeling approach

2.2.1. Summary of the WEPP model

The WEPP is a physical model for simulating soil water erosion and Run-off, developed by the USDA-ARS and initiated in 1985 (Nearing, 1998). The model assesses the impact of various landscape factors on soil erosion and Run-off, such as soil properties, infiltration theory, land cover, land management, along with stochastic weather generation (rainfall characteristics and evapotranspiration) (Meinen, & Robinson, 2021). It has been successfully implemented in many parts of the world under different climatic conditions and land uses, such as the USA (Flanagan et al., 2007), China (Zhu et al., 2023), Syria (Mohammed et al., 2021b), and many others. The WEPP model accounts for calculating the amount of eroded soil accumulated at the outlet on a daily basis from rill and inter-rill erosion.

The WEPP model adopts a two-state Markov chain for generating the number and distribution of precipitation events, where 12 monthly values representing the probabilities of wet and dry events account for transitions from one season to another. The daily rainfall is then calculated using an equation (1) that forms a skewed normal distribution (Flanagan, & Nearing, 1995, Chen et al. 2009).

$$\boldsymbol{x = \frac{6}{g}\left\{\left[\frac{g}{2}\left(\frac{R-u}{s}\right)+1\right]^{\frac{1}{3}}-1\right\}+\frac{g}{6}} \qquad (\mathbf{1})$$

where: x: the standard normal deviate, R: the daily precipitation, g: skew coefficient, u: mean, s: standard deviation.

For soil sediment movement, the WEPP model employed the steady-state sediment continuity equation:

$$\frac{dG}{dx} = D_f + D_i \quad (2)$$

where: G (kg. s $^{-1}$. m^{-1}): soil sediment, x (m): distance, D_f (kg. s $^{-1}$. m^{-2}): rill erosion rate, D_i (kg. s $^{-1}$. m^{-2}): inter-rill sediment delivery to the rill.

Run-off is one of the complex processes that need to be carefully modelled. The modeling approach that adopted by WEPP model includes four different steps: calculation of soil infiltration, then rainfall excess, followed by depression storge, and peak discharge (Shen et al., 2009). Based on that, the WEPP model combines two equations for accurately predict run-off Run-off the Green-Ampt Mein-Larson (GAML) model (equation (3)) with a kinematic wave model (KWM) (equation (4)) (Flanagan & Nearing, 1995). The GAML is used to predict infiltration over time taking into consideration rainfall events, while the KWM is used to determine the peak discharge of the run-off hydrograph (Flanagan & Nearing, 1995, Miller, 1984).

$$f_{inf,t} = K_e \left(1 + \frac{\Psi_{wf} \Delta\emptyset_v}{F_{inf,t}}\right) \quad (3)$$

where: $f_{inf,t}$ (mm h^{-1}): infiltration rate by time (t); K_e (mm h^{-1}): effective hydraulic conductivity; Ψ_{wf} (mm): the matric potential of wetting front; $\Delta\emptyset_v$ (dimensionless): changes in the volumetric moisture, $F_{inf,t}$ (mm): cumulative infiltration.

$$\frac{\partial h}{\partial t} + \frac{\partial q}{\partial x} = 0 \quad (4)$$

where: h (m): flow depth; q (m^3. m^{-1}. s $^{-1}$): discharge; X (m): distance.

2.2.2. **Model Input Variables**:

To run the WEPP model, observed data were collected and prepared for simulation. Four different categories of files/data needed to be prepared to run the model, which include climate data, soil data, topographical (slope) data, and management data. Observed daily temperature (maximum and minimum) and daily rainfall from 2010 to 2019 were prepared and uploaded to the model. In this context, the WEPP model incorporates a climate generator program called CLIGEN

(version 4.3) (Nicks et al., 1995), which can produce the necessary climatic data based on the uploaded climatic parameters. After uploading the climatic data, CLIGEN was activated, and the climate data were set up for the entire study area. Subsequently, the model was run to produce estimates for a 20-year period (2020-2040). Slope profile files and soil database were entered into the model based on the collected data (**Table 1**). Consequently, four soil files and four slope files were created, each representing one studied location. For management file, the input setup was chosen to represent the land use within each location. Thus, the management WEPP file "winter wheat, conventional till", was utilized for *KS* location; "Winter Wheat-no till" for *MN*, "Forest" for *AINF* and "Forest/30% covered after fire" for *AINBF*. Interestingly, Interestingly, all selected files were carefully checked to ensure the compatibility of sub-criteria with the study area. For instance, parameters related to wheat, such as sowing and harvesting, were adjusted to fit the study area. Additionally, the forest files were also reviewed. In summary, one climate file was prepared, along with another 12 files for the combination of 4 locations (KS, NM, AINF, AINBF) and 3 types of input data (management, soil, slope).

2.2.3. Model calibration and prediction steps

By using data from 27 locations distributed across different agro-ecosystems, namely agricultural land, forest, and burned forest, and spanning different topographical gradients from 10% to 50%, the WEPP model was calibrated and assessed. Published results indicated that the WEPP model was efficient in predicting erosion and run-off in both agricultural lands and burned forests, while it was less efficient in forest systems (Mohammed et al., 2021b). More details are available in Mohammed et al. (2021b,c).

Previously, it was reported that parameters such as effective hydraulic conductivity (mm/h), critical shear stress (Pa), rill erodibility (m/s), and inter-rill erodibility (kg.s/m^{-4}) play crucial roles in the WEPP model sensitivity analysis (Wang et al., 2023). These parameters can be adjusted to optimize the WEPP model's performance through sensitivity evaluation. However, due to the model's acceptable performance, the sensitivity analysis process was not conducted. Instead, we opted for the WEPP model's built-in option, "Have Model Calculate," to automatically determine these values.

After preparing the input files, the WEPP model was run for each study location. Then, predicted data were collected and compared with the observed one. Finally, the model was run to simulate

the erosion process within the study area for twenty years (2020-2040). The extracted data includes daily soil moisture (θ), soil water erosion (SE), run-off (RF), and hydraulic conductivity (K_{sw}).

2.2.4. Assessment model performance in predicting SE and RF

To assess the WEPP model's performance, four statistical indicators were utilized. Namely, model efficiency (NSE), the model ratio of mean square error to standard deviation of observed data (RSR), % of bias (PBIAS), and coefficient of determination (R^2) (**Table 2**). Also, a Taylor diagram was plotted to illustrate the model performance in comparison with measured data in terms of correlation, mean square error, and standard deviation.

Table 2. Evaluation of the WEPP model's performance (Saghafian et al. 2015)

Indicator	Equation	No.	Range	Evaluation
NSE	$\boldsymbol{NSE} = \mathbf{1} - \frac{\sum_{i=1}^{n} (\nabla_{obs} - \hat{\nabla}_{WEPP})^2}{\sum_{i=1}^{n} (\nabla_{obs} - \bar{\nabla}_{obs})^2}$	**(5)**	0 to ∞	Very Good: NSE > 0.75; Good: 0.65 < NSE ≤ 0.75; Satisfactory: 0.50 < NSE ≤ 0.65; Unsatisfactory: NSE ≤ 0.50
RSR	$\boldsymbol{RSR} = \frac{\sqrt{\sum_{i=1}^{n} (\nabla_{obs} - \hat{\nabla}_{WEPP})^2}}{\sqrt{\sum_{i=1}^{n} (\nabla_{obs} - \bar{\nabla}_{obs})^2}}$	**(6)**	0 to ∞	RSR ≤ 0.50: very good; 0.50 < RSR ≤ 0.60: good; 0.60 < RSR ≤ 0.70: satisfactory; >0.7: unacceptable.
$PBIAS$	$\boldsymbol{PBIAS} = \frac{\sum_{i=1}^{n} (\nabla_{obs} - \hat{\nabla}_{WEPP})}{\sum_{i=1}^{n} (\nabla_{obs})}$	**(7)**	−∞ to +∞	ER: Very Good: PBIAS < ±15; Good: ±15 ≤ PBIAS < ±30; Satisfactory: ±30 ≤ PBIAS < ±55; Unacceptable: PBIAS ≥ ±55. RF: Very Good: PBIAS < ±10; Good: ±10 ≤ PBIAS < ±15; Satisfactory: ±15 ≤ PBIAS < ±25; Unacceptable: PBIAS ≥ ±25.
R^2	$\boldsymbol{R^2} = \mathbf{1} - \frac{\sum_{i=1}^{n} (\nabla_{WEPP} - \bar{\nabla}_{obs})^2}{\sum_{i=1}^{n} (\nabla_{obs} - \bar{\nabla}_{obs})^2}$	**(8)**	0-1	0: very poor 1: perfect fit

∇_{obs}: observed value, $\hat{\nabla}_{WEPP}$: predicted value, $\bar{\nabla}_{obs}$: average.

2.3. Statistical analysis

For statistical analysis, the Tukey-HSD test was employed to compare the mean differences between the output of the four studied locations. The Tukey test is one of the parametric method the compare all possible pairs, which assumes the homogeneity of variance and normal distribution of the tested data.

Furthermore, the SE and RF magnitude was calculated by using the following equation.

$$\nabla = \left(\sum_{j=1}^{x} \partial_{i,j}\right) \ldots \ldots \ldots \ldots \ldots \ldots \ldots \ldots \ldots \ldots \ldots \ldots \ldots \ldots \ldots \ldots \ldots \ldots \ldots \ldots . \ldots . (9)$$

Where j stands for the first month of the 20 years and continues till the end of event x for the time scale i for the whole predicted period. The sum, which represents the magnitude was categorized into four groups: normal, moderate, high, and extreme.

To summarize the predicted data derived from the four studied locations (2020-2040), which include daily soil moisture (θ), soil water erosion (SE), run-off (RF), and hydraulic conductivity (K_{sw}), Principal Component Analysis (PCA) was used. PCA is a statistical parametric method that summarizes the original dataset into a smaller number of orthogonal principal components (PCs). This method is classified under the dimension reduction technique which all to retaining the variability of the original dataset as possible. Hence, PCs simplify the dataset in an effective and sound way by capturing the underlying pattern and relationship within the dataset to simplify the analysis of complex dataset.

3. Results

3.1. Applicability of WEPP model in predicting soil erosion and Run-off in the eastern Mediterranean (2019)

To address the applicability of WEPP model, observed data were compared with predicted data by using a set of indices. Results showed that the model performs well in predicting both soil erosion and Run-off. The coefficient of determination (R^2) reached 0.97 for predicting soil erosion and 0.78 in predicting run-off (Fig 2 a,d). NSE results revealed a good performance, with almost the same values for RF and SE reaching 0.66 and 0.67, respectively (Fig 2 b). Same outputs were recorded from RSR, where for both RF and SE, the indicator was 0.57 and classified as good, indicating a good model performance (Fig 2 f). The Taylor diagram showed that the predicted value of SE was on the 0.99 correlation coefficient line with 1 standard deviation (Fig 2 c), while

the RF was on 0.9 correlation coefficient line with 50 standard deviation (Fig 2 g). However, both RF and SE were in good agreement and close to the observed data.

In a location scale, the WEPP model tends to underestimate soil erosion and run-off in most of the locations. For instance, the observed SE in MN and KS was 0.96±0.04 and 4.4±0.12 kg/m^2, respectively, while the predicted values were 0.45 and 2.53 kg/m^2. Similarly, for AINBF and KS locations, the observed RF was 175±3.25 and 280±3.8 mm, respectively, while the predicted ones were 175 and 276 mm.

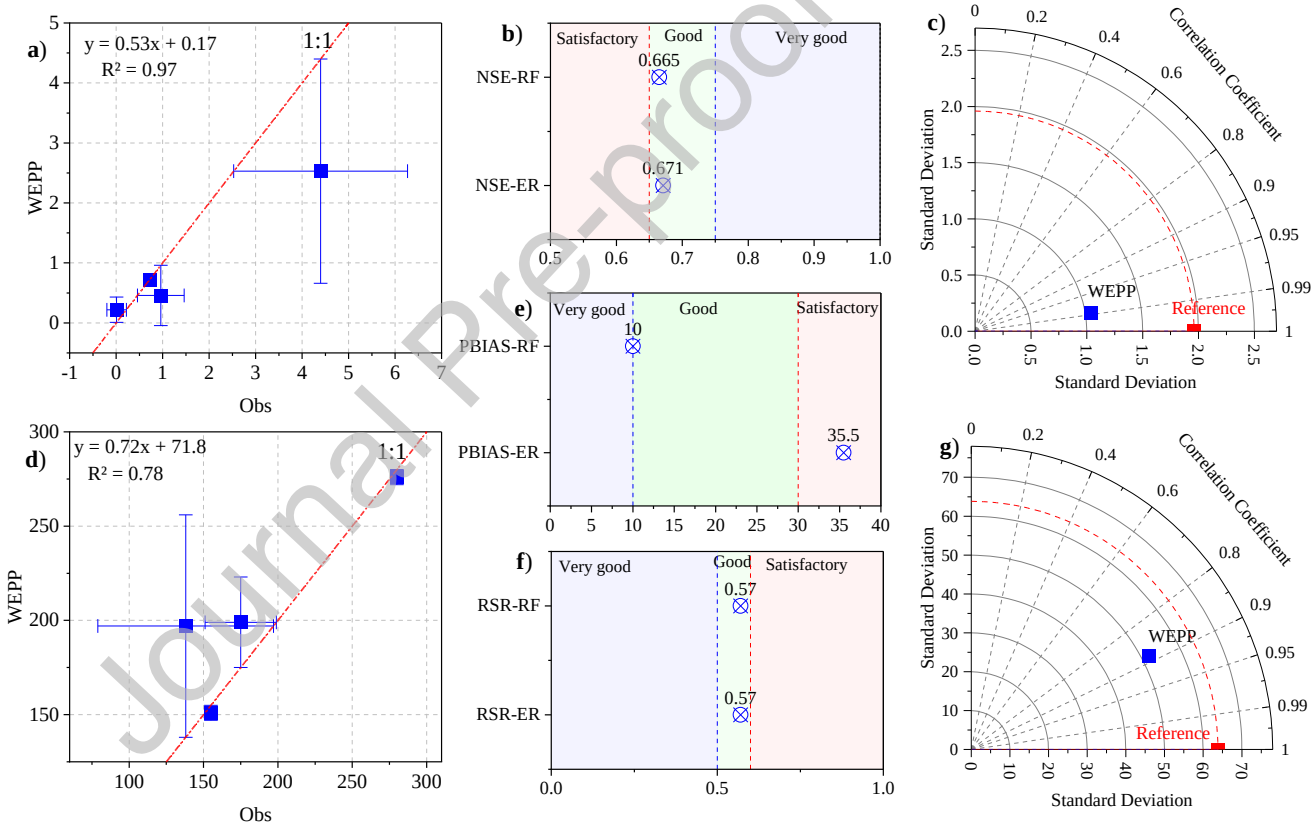

Fig. 2: WEPP model performance in predicting (Obs.) soil erosion and Run-off: a) scatterplot SE, b) NSE, c) Taylor diagram SE, d) scatterplot RF, e) PBIAS, f) RSR, g) Taylor diagram RF.

3.2.An overview of event-by-event prediction by WEPP (2019)

The WEPP model provides a detailed forecast of rainstorms (mm) for specific days using a two-state Markov chain and predicts the corresponding Run-off(mm) and soil erosion (kg/m^2). In this context, the WEPP model forecasted 19 rainfall events spanning from 01/01/2019 (25 mm) to 24/12/2019 (39.1 mm) (Fig 2 a). The highest accumulated rainstorm (R-max) was on 09/01/2019 (134 mm), while the lowest 04/12/2019 (9.3 mm) (R-low). In this analysis, the correspondence RF within R-max varied across locations, with RF predicted to be 68.1, 61, 64, 72.5 mm (Fig 2 b); and SE 0.194, 0.16, 0.083, 0.322 kg/m^2 (Fig 2 c), at KS, MN, AINF, and AINBF, respectively. On the other hand, the RF within R-low was 1, 1.8, 0.5, 0 mm, and SE was 0.002, 0.001, 0, 0 kg/m^2 (Fig 2 c), at KS, MN, AINF, and AINBF, respectively. Notably, three storms were only able to generate run-off and erosion in KS, while it had no effect on other locations due to varying land use and land cover.

The correlation analysis between predicted rainfall events, RF and SE showed strong and significant relationships. The correlation coefficient (r) reached 0.94 ($p<0.05$) between RF and rainfall (Fig 2 d), $r=0.81$ ($p<0.05$) ER vs. rainfall (Fig 2 e), and $r=0.88$ ER VS SE (Fig 2 f). These high correlations between different outputs indicate significant, and robust model output.

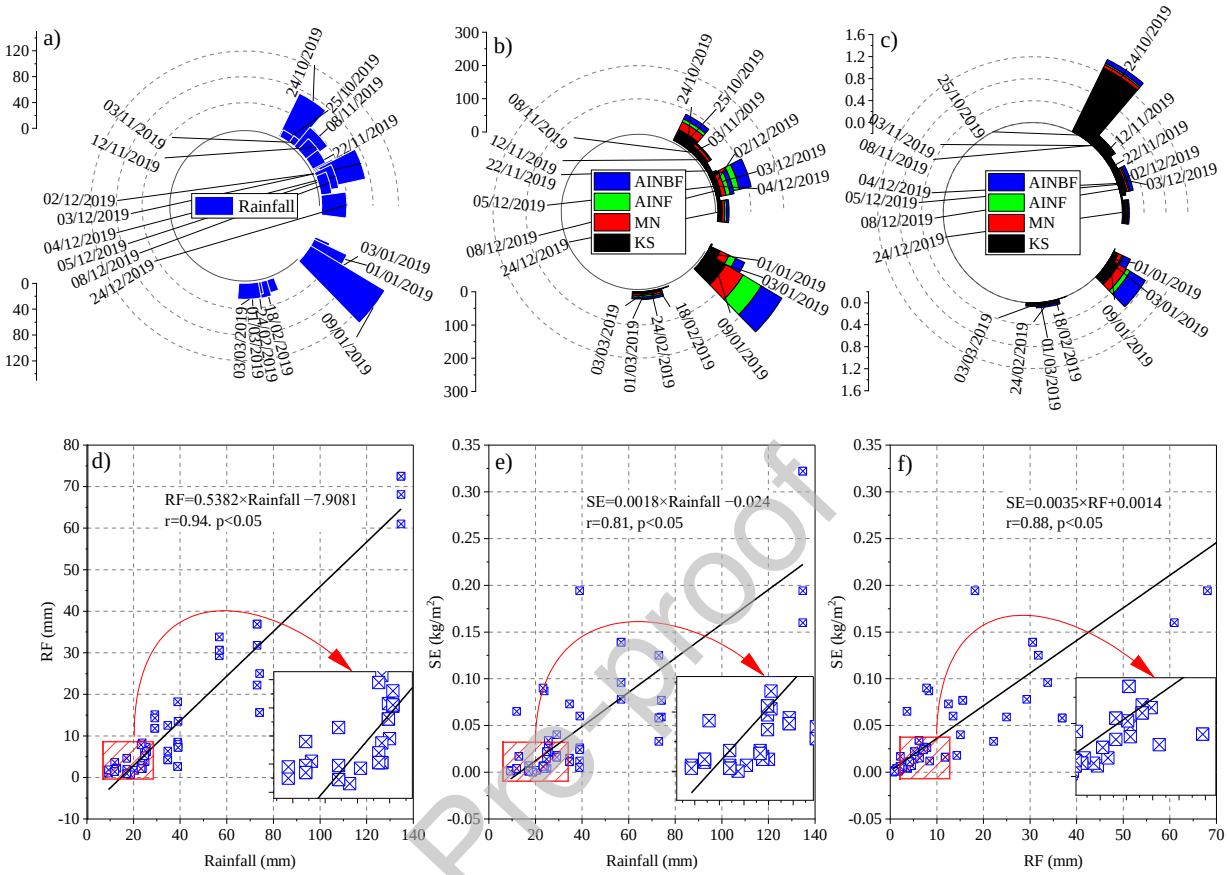

Fig. 3: Predicted events by WEPP model for 2019: a) forecasted rainfall, b) predicted RF, c) predicted SE, d) scatter plot for RF and rainfall, e) scatter plot for SE and rainfall, and f) scatter plot for RF and SE. (black line linear regression, red box represents zoom on to group of data)

3.3.Forecasting future climate variables within the study area (2020-2040)

The WEPP model was initially operated using the observed climate data (2010-2019). Subsequently, the climate generator program (CLIGEN) was used to generate future climatic variables for the subsequent 20 years (2020-2040). A comparison between the observed data and forecasted one will provide insights into potential climate change in the study area.

Analysis of observed monthly rainfall data (2010-2019) revealed that the highest rainfall occurred in January (199.71±29.53 mm), followed by December (165.3±108.69 mm) (Fig 4 A,

blue line). However, during the summer season no rainfall was recorded (Fig 4 A, blue line). The forecasted rainfall data largely aligns with historical monthly rainfall, with notable differences occurring from September to December (Fig 4 A, red line). The average total rainfall in January (2020-2040) was projected at 190.69±70.10 mm, while in December was predicted at 142.93±69.10 mm. The output of Tukey test revealed that no significant differences in the mean yearly rainfall between the historical data and forecasted one (Fig 4 B). However, total annual forecasted rainfall ranged from 800 to 1200 mm, (Fig 4 C).

In terms of max temperature (T_{max}), the monthly averages of observed and forecasted data showed minimal variation (Fig 4 D). Slight differences occurred from March to May and in December, where the predicted average T_{max} (red line) was marginally higher than the historical (blue line) (Fig 4 D). The Tukey test revealed no significant difference between the modeled mean T_{max} (24.7±0.21 °C) and the observed one (24.7±0.59 °C) (Fig 4 E). Nevertheless, the average annual T_{max} for the future predicted data ranged from 24.2 °C to 25.5 °C (Fig 4 F).

For the minimum temperature (T_{min}), minor differences in the average monthly temperature were observed, especially from January to May (Fig 4 G). These differences were statistically significant according to the Tukey's HSD test, where the monthly average forecasted T_{min} (15.12±0.9 °C) was significantly lower than the current observed one (16.12±0.44 °C) (Fig 4 H). However, a noticeable decreasing trend in T_{min} is evident, especially after 2035 (Fig 4 I).

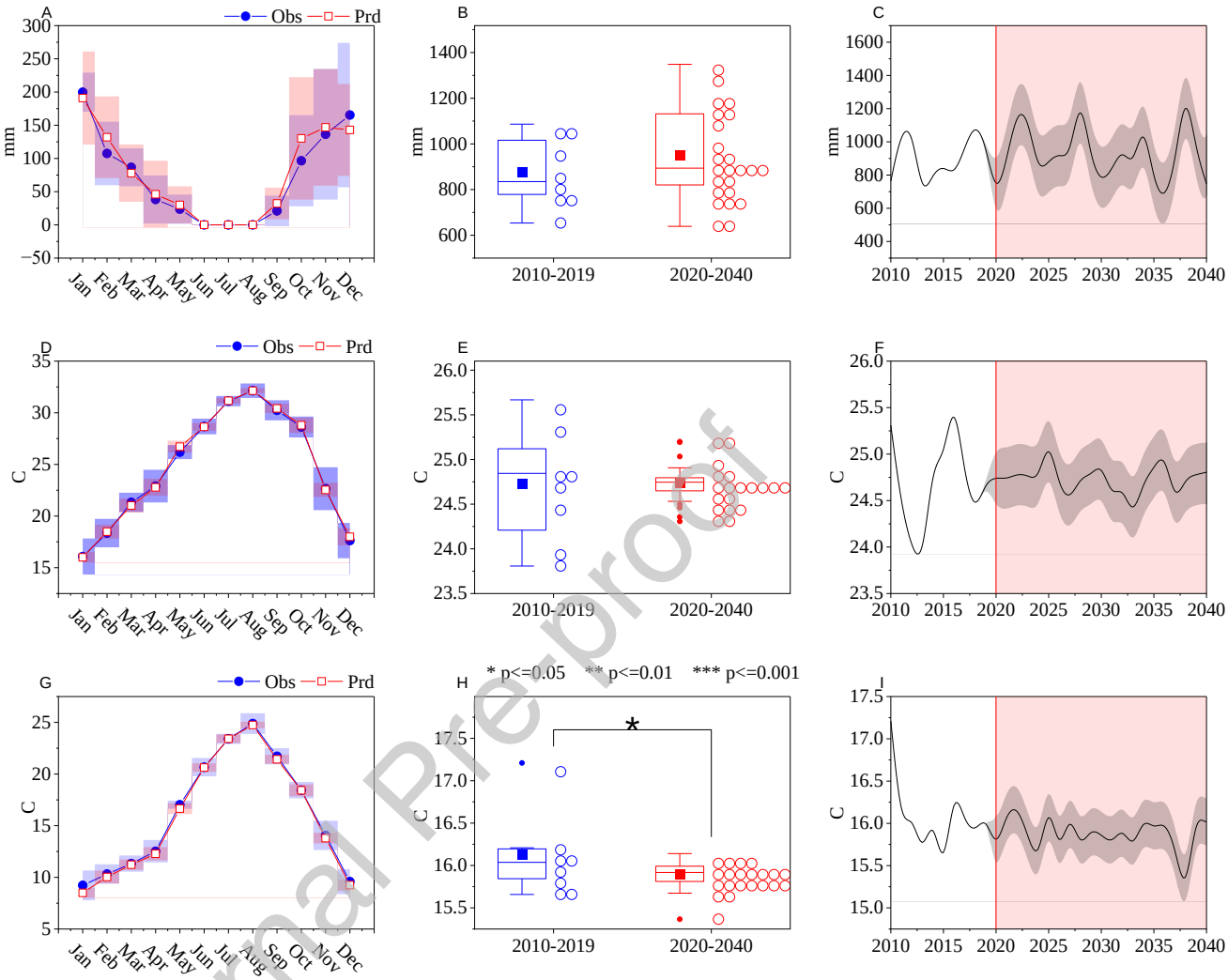

Fig. 4: Observed (Obs.) climate variables and forecasted (Prd) one by WEPP model from 2010 to 2040: a) observed (2010-2019, blue line) and predicted (2020-2040, red line) monthly rainfall, shadow colors represented the stander deviation, b) boxplot of Tukey test for monthly rainfall: observed (2010-2019) vs predicted (2020-2040), c) time line of yearly rainfall data (2010 to 2040), red shadow represents the predicted period (2020-2040), gray shadow represents the yearly rainfall stander deviation, D) average observed (2010-2019) and predicted (2020-2040) monthly T_{max}, shadow colors represented the stander deviation, E) boxplot of Tukey test for average yarely T_{max}: observed (2010-2019) vs predicted (2020-2040), F) time line of average yearly T_{max} data, red shadow represents the predicted period (2020-2040), gray shadow represents the T_{max} stander deviation, G) average observed (2010-2019) and predicted (2020-2040) monthly T_{min}, shadow colors represented the stander deviation, H) boxplot of Tukey test for average yearly T_{min}: observed (2010-2019) vs predicted (2020-2040), I) time line of average yearly T_{min} data, red shadow represents the predicted period, gray shadow represents the T_{min} stander deviation.

3.4. **Future prediction of Run-off and soil water erosion on an annual scale**

The future response of different ecosystems to run-off and soil water erosion was analyzed. Results demonstrated dynamic interactions among different locations, with both run-off and soil water erosion. For RF and SE, a decreasing trend was observed compared to the base line state of 2019 (Fig 5 a,b). Among all locations, KS responded with the highest predicted run-off in all years, exceeding 250 mm threshold in some years (Fig 5 a). The peak run-off was predicted in 2025, with an estimate of 411.17 mm. In contrast, the lowest RF was recorded in 2019 at AINF location (155 mm, the base line). However, future forecasts showed that the AINBF will experience the lowest predicted Run-off, ranging from 199 in 2019 to 131.1 mm in 2038. Notably, in the AINBF, AINF, and MN locations, RF did not exceed 150 mm (Fig 5 a). Similarly, SE corresponds to the results of RF, with the highest values projected for the KS locations (Fig 5 b, black dot). Where, in all years, the SE exceeded 1 kg/m^2 in both baseline and future projected erosion (Fig 5 b, black dot). In contrast, at the remaining three locations, despite varied response to predicted SE, the SE remained less than 0.5 kg/m^2 (Fig 5 b). The highest recorded SE value was 5.89 kg/m^2 in the year 2025 at the KS location, while the lowest projected SE value was 0.087 kg/m^2 recorded at AINBF in 2038.

As each ecosystem responded differently to both RF and SE, it is essential to compare the means to reveal if significant differences exist. According to the Tukey's HSD test, statistically significant ($p<0.05$) differences between the KS location and other locations was captured, for both RF and SE (Fig 5 c, d). However, no significant differences were observed among the other three locations among themselves (i.e., AINBF, AINF, and MN). For RF, the locations can be ranked as: KS (234.7mm±75.6)> MN (141.1mm±50.2)> AINF (145.4mm±47.4) > AINBF (100.3mm±49.2). While for SE, the locations can be classified as: KS (2.38 kg/m^2 ±1.36)> AINF (0.45 kg/m^2 ±0.17) > MN (0.31 kg/m^2 ±0.11)> AINBF (0.24 kg/m^2 ±0.15). Overall, in the three studied ecosystems, a decreasing trend of both RF and SE was observed comparing with the baseline (Fig 5 e, f).

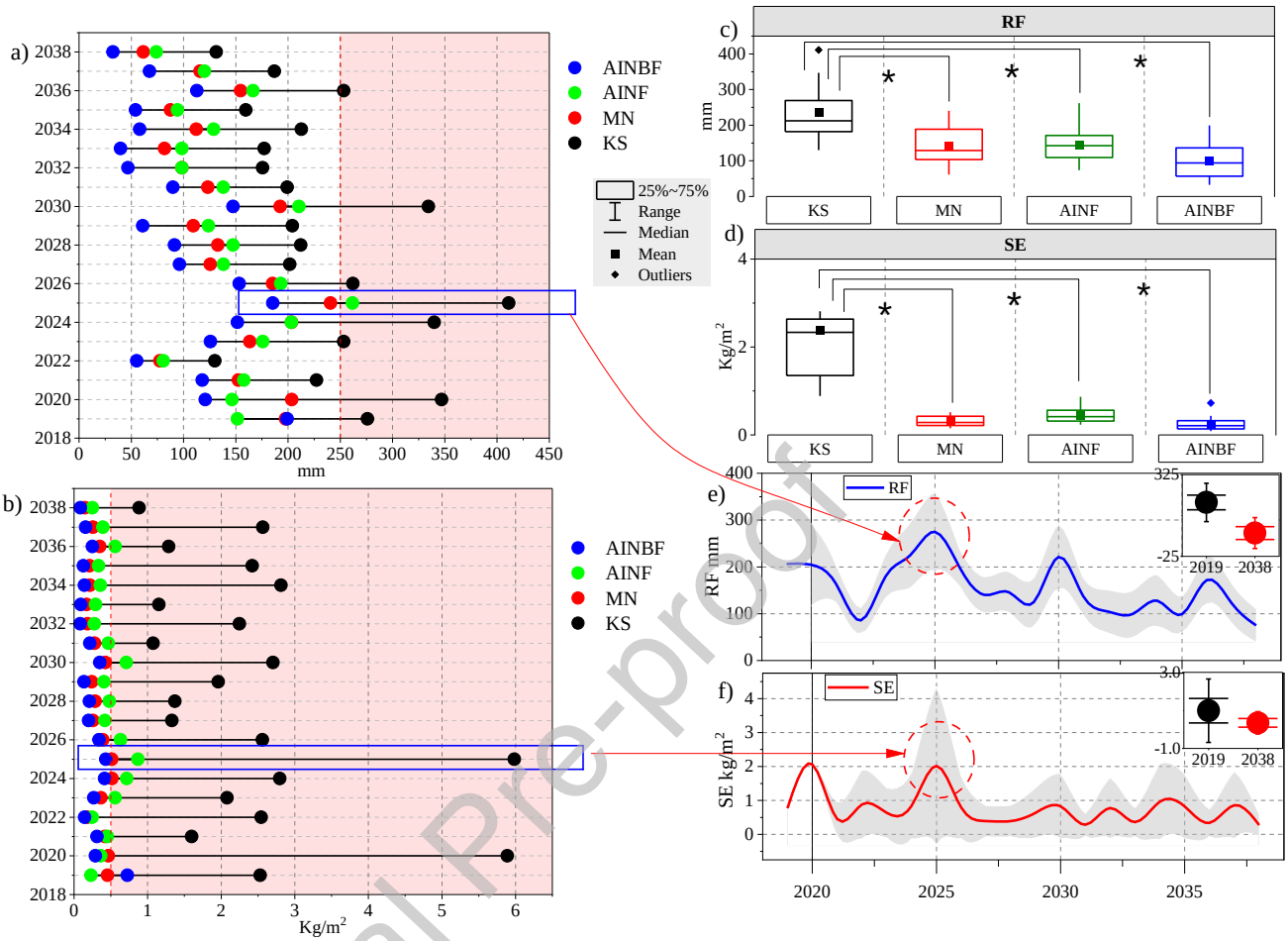

Fig. 5: An overview of future prediction of run-off and soil water erosion on an annual scale in the four studied locations: a) predicted annual RF from 2019 to 2038 (red shadow represents 250 mm threshold), b) predicted annual SE from 2019 to 2038 (red shadow represents 0.50 kg/m^2 threshold), c) results of Tukey's HSD test for predicted annual RF within the four locations (★ represents the significant differences ($p<0.05$)), d) results of Tukey's HSD test for predicted annual SE within the four locations (★ represents the significant differences ($p<0.05$)), e) average annual RF within the study locations (gray shadow represents standard deviation, and f) average annual SE within the study locations (gray shadow represents standard deviation).

3.5.Detailed analysis of parameters related to predicted soil erosion process on a monthly scale

Exploring erosion processes on a monthly scale can significantly enhance the overall understanding of these processes, improving the reliability of the model, and their response to projected scenarios. In this context, Fig. 6 displays four key parameters run-off (RF, mm), soil erosion (SE, kg/m^2), soil water content (θ, %), and soil water hydraulic conductivity (K_{sw}, mm/hr),

across three studied ecosystems from 2019 (base line) to 2038. Previous results on an annual scale revealed that the highest RF and SE (Fig 5 a,b) was recorded in the KS, a monthly breakdown provides a deep understanding for the process that lead to this outcome. A detailed review of Fig.6-a, and Fig.6-b showed that RF and SE at the KS location (black line/column) consistently exceeded those of other locations. For instance, the highest accumulated RF value was predicted to be in October reaching 142.6 mm, and the corresponding SE was 5 kg/m^2. In contrast, in the same month, RF was predicted to be 78.5, 61.7, 60.3 mm for MN, AINF, and AINBF respectively, with corresponding SE values of 0.1, 0.2, 0.2 kg/m^2.

Soil water content is an important factor for determining soil moisture and its consequences on erosion process. Given the Mediterranean climate of the study area, θ reflects seasonal climatic conditions, where high values expected in rainy season and low values during dry summer. Fig.6-c reflects the monthly forecasted changes in θ, with the highest values recorded at 65.34% in February 2035 for KS, 78.99% in February 2035 for MN, 82.61% in January 2021 for AINF, and 72.63% in February 2035 for AINBF. While the lowest θ values occur during summer season (June to August), reaching 46.3%, 50.3%, 46.2%, and 49.2%, for KS, MN, AINF, and AINBF, respectively. Tracking the variation of θ across these study locations showed a seasonal pattern, increasing during fall and winter seasons and direct decreasing in spring and summer seasons, mainly summer, as can be seen clearly in Fig.6-c. However, the ecosystem's response varies, in KS (black line), a notable sharp decrease in θ during summer is observed due to agricultural activities that leave the soil bare and directly exposed to solar radiation which accelerate evapotranspiration process. In contrast, other locations demonstrate more resilient θ fluctuation. In this context, the projected θ of AINF (green line) was the highest, which could be explained as this location represent forest ecosystem, with rich in organic matter promoting water absorption and increasing field capacity. Additionally, the forest canopy adequately blocks most solar radiation thus protecting the soil moisture. It's worth to mention that the patterns of θ within AINF and AINBF are similar, while KS and MN are closer to each other, which directly reflects the impact of soil management.

The case of K_{sw} is opposite to θ, where the highest K_{sw} was observed and predicted in summer and the lowest in winter (Fig.6-d). At the KS location, K_{sw} ranged from 1.3 to 6.3 mm/hr, with an average of 2.29±1.3 mm/hr. This variation can be noticed clearly by tracking the black line (Fig.6-d), which indicates a decreasing K_{sw} during rainy season, while peaking in dry season due to low

soil moisture and empty soil pores. Conversely, the variations in K_{sw} was less pronounced for rest locations, where the average of K_{sw}: 3.93±0.5 mm/hr, 3.09±0.6 mm/hr, and 3.17±0.6 mm/hr, for MN, AINF and AINBF, respectively (Fig.6-d). Interestingly, the projected data showed that the K_{sw} pattern of MN (red line), AINF (green line), and AINBF (blue line) were closely aligned (Fig.6-d 1&2).

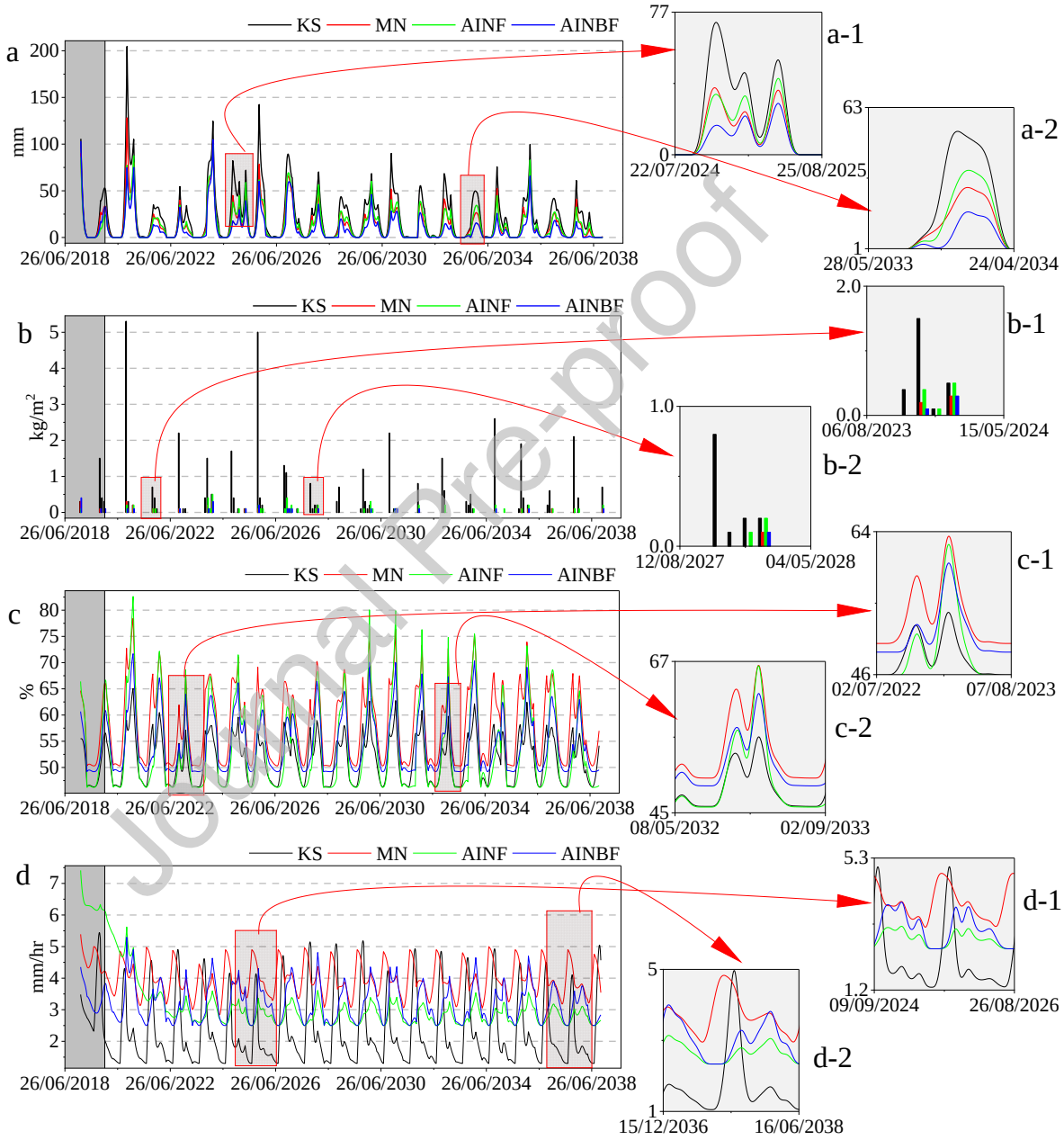

Fig. 6: Timeline illustrating the WEPP model's forecasted monthly results for selected parameters across three studied ecosystems, from 2019 (base line) to 2038: a) Run-off (RF, mm) with zoom

in to: a-1) 07/2024-08/2025; a-2) 05/2033-04/2034, b) soil erosion (SE, kg/m^2) with zoom in to: b-1) 08/2023-05/2024; b-2) 08/2027-05/2028, c) soil water content (θ, %) with zoom in to: c-1) 07/2022-08/2023; c-2) 05/2032-09/2033, and d) soil water hydraulic conductivity (K_{sw}, mm/hr) with zoom in to: d-1) 09/2024-08/2026; d-2) 12/2036-06/2038. (Gray color represents the baseline).

The PCA analysis revealed that the PC1 accounted for 56.2% of the total variance, while the PC2 for 14.3%, in total 70.44%. (Fig.7-a). The eigenvalue of PC1 was 8.9, followed by 2.2 for PC2 (Table 3). The output revealed that RF had positive correlation with PC1, with loading between 0.317 and 0.306. On the other hand, SE had a positive correlation with PC2, where the loadings ranged between 0.19 and 0.34. However, Fig.7-a illustrated that SE and RF positively influenced each other, located in the upper quartile of the diagram (+, +). While K_{sw} and θ located on the third quartile (+, -), indicating inverse relationship, where an increase in one directly lead to a decrease in another factor (Fig.7-a). Network analysis of the four monthly studied ecosystem parameters reveled a positive correlation between SE and RF, RF and θ, and a negative correlation between SE and K_{sw} (Fig.7-b).

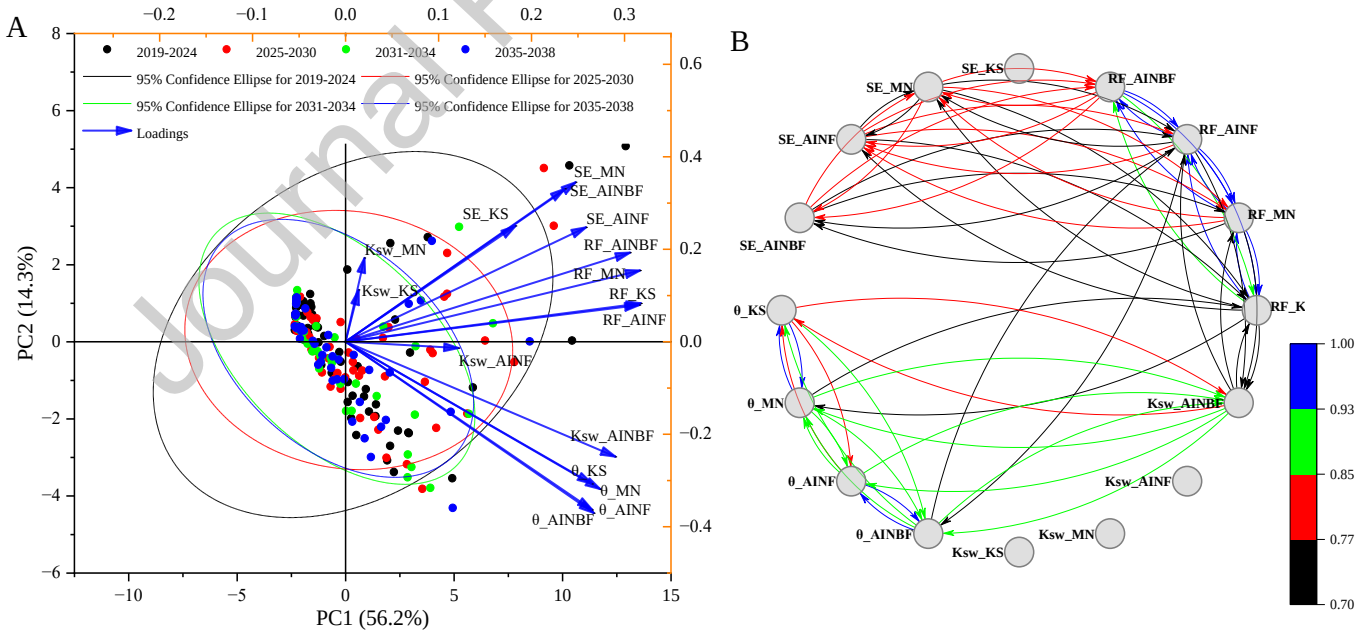

Fig. 7: PCA and Network analysis diagrams depicting the WEPP model's forecasted monthly results (2019-2038) for selected parameters across three studied ecosystems: A) PCA diagram, and B) Network analysis diagram.

Table 3: PCA analysis for predicted some ecosystem parameters related to soil water erosion in four different ecosystems in eastern Mediterranean.

PC Number	Eigenvalue		PC1 (56.2%)	PC2 (14.3%)
Eigenvalues		**Loadings**		
1	8.98939	RF_KS	**0.31632**	0.07938
2	2.28227	RF_MN	**0.31696**	0.15407
3	1.50661	RF_AINF	**0.31792**	0.08299
4	1.00715	RF_AINBF	**0.30618**	0.19276
5	0.79377	SE_KS	0.18303	0.2507
6	0.54023	SE_MN	0.24763	**0.34511**
7	0.28852	SE_AINF	0.25888	0.2475
8	0.2213	SE_AINBF	0.23617	**0.33106**
9	0.12952	θ_KS	0.26535	-0.30727
10	0.11131	θ_MN	0.27395	-0.31862
11	0.07664	θ_AINF	0.26546	-0.36367
12	0.02487	θ_AINBF	0.26715	-0.37068
13	0.01034	K_{sw}_KS	0.01421	0.11233
14	0.00856	K_{sw}_MN	0.02042	0.18138
15	0.00576	K_{sw}_AINF	0.12168	-0.01372
16	0.00377	K_{sw}_AINBF	0.29038	-0.24863

3.6. Intensity and magnitude of selected erosion parameters (2019-2038)

Summarizing the dynamic response of the studied ecosystems through selected erosion parameters provides an overview of the intensity of each parameter each year. Fig 8-A illustrates the 2D Kernel density of each parameter-total rainfall (mm), average monthly run-off (RF, mm), average monthly soil erosion (SE, kg/m^2), average monthly soil water content (θ, %), and average monthly soil water hydraulic conductivity (K_{sw}, mm/hr)- across four ecosystems from 2019 (base line) to 2038 on a monthly scale. Where, the average monthly values represent the average of each parameter across the four ecosystems in each month. This approach, integrating 2D Kernel density, captures the spatial and temporal fluctuation of these parameters. Fig.8-A (1) shows that all ecosystems have a minimum rainfall 0-20 mm, depicted in blue, reaching a peak density 0.14, with the majority receiving rainfall less than 200 mm. Notably, some years, like 2025, reached the highest extent, but the Kernel density remained low (0.07), reflecting low occurrence of such extreme values. RF fluctuated from 1 to 22 mm in most years, but some years experienced high run-off volume exceeding 50 mm, however these events are less likely to occur (Fig.8-A (2)). For

SE most of the predicted erosion was less than 0.5 kg/m^2 per month, with exceptional peaks in 2025 and 2035(Fig.8-A (3)). In terms of soil water content θ, majority of the years exhibited values less than 50% (density 0.27), with a notable proportion ranging from 50% to 80%; but with less density (0.19) (Fig.8-A (4)). Finally, the average K_{sw} values reflected the dominant value in the eastern Mediterranean ranges from 2 to 4 mm/hr with high Kernel density reaching 0.39 (Fig.8-A (5)).

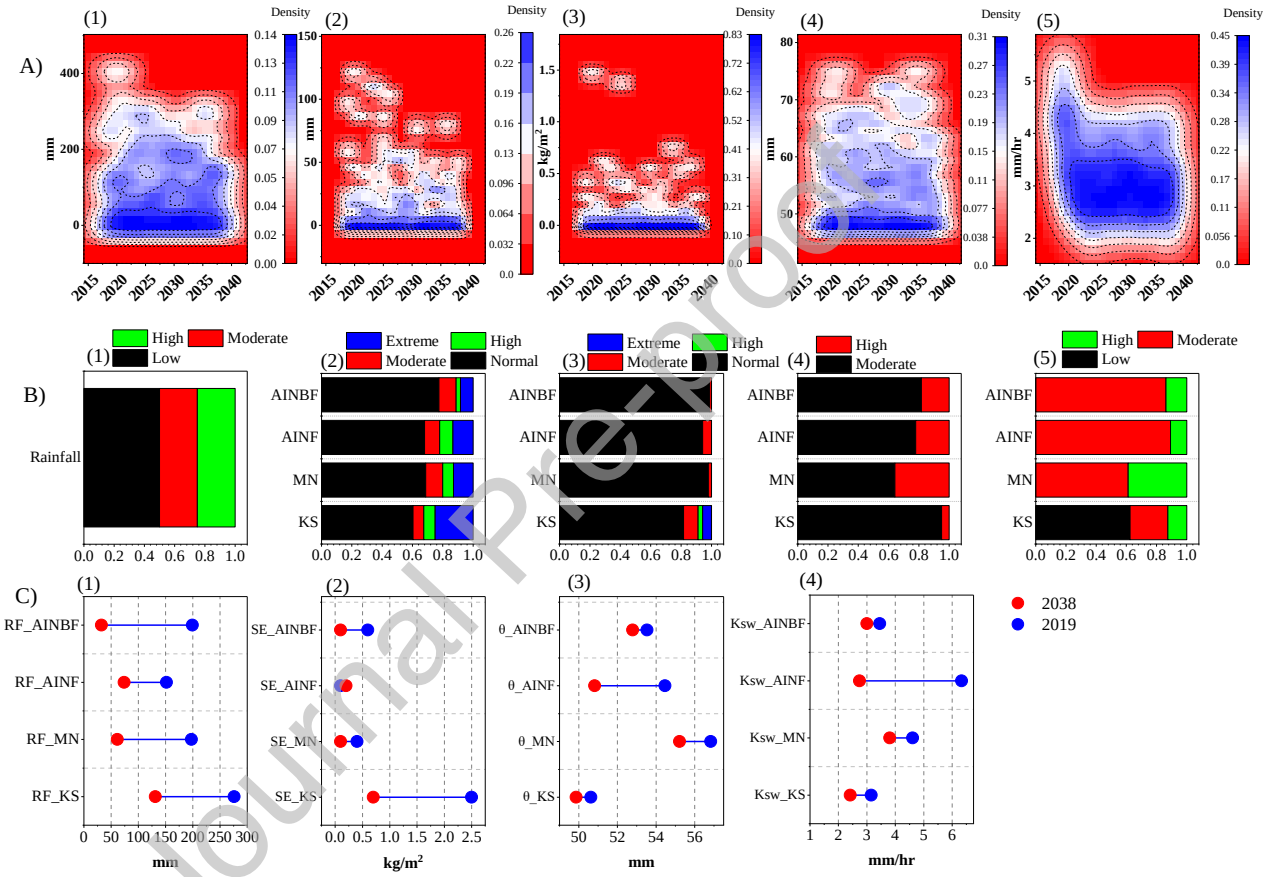

Fig. 8: Intensity and magnitude of forecasted WEPP model from 2019 to 2038: A) average monthly 2D Kernel density for: 1) rainfall (R, mm), 2) Run-off(RF, mm), 3) soil erosion (SE, kg/m^2), 4) soil water content (θ, %), 5) average monthly soil water hydraulic conductivity (K_{sw}, mm/hr); B) magnitude of selected erosion parameters (2019-2038): 1) R, 2) RF, 3) SE, 4) θ, 5) K_{sw}; C) Changes between baseline values in 2019 and the forecasted WEPP model values for the year 2038: 1) R, 2) RF, 3) SE, 4) θ, 5) K_{sw}.

Analyzing the future magnitude of the forecasted results provides insights into the intensity of each parameter. For forecasted rainfall data, 50% of the events were low (≤ 45 mm/month), 25% were

moderate (> 45 mm/month and ≤ 126.1 mm/month), and 25% were high (> 126.1 mm/month) (Fig.8-B (1)). The response to predicted run-off fof varied across ecosystems. For instance, in the KS location, 60.42 % of events were classified as normal (≤ 10.0 mm), 7.08% as moderate (> 10.0 and ≤ 20 mm), 7.50% as high (> 20 and ≤ 30.7 mm), and 25.00% as extreme (> 30.7 mm). In MN the results were distributed as 68.75% normal, 11.25% moderate, 7.08% high, and 12.92% extreme. In AINF the results were distributed as 67.92% normal, 10.00% moderate, 8.75% high, and 13.33% extreme. While in AINBF, the results were distributed as 77.50% normal, 11.25% moderate, 2.92% high, and 8.33% extreme (Fig.8-B (2)). Soil erosion results were more intense in KS location and less pronounced in the rest of the studied locations. Here, 81.67% of events were normal (≤ 0.1 kg/m^2), 9.58% moderate (> 0.1 and ≤ 0.5 kg/m^2), 2.92% high (> 0.5 and ≤ 1.0 kg/m^2), and 5.83% extreme (> 1.0 kg/m^2) (Fig.8-B (3)). For soil water content, all of locations exhibited moderate to high values (Fig.8-B (4)). Finally, soil water hydraulic conductivity varied between ecosystems (Fig.8-B (5)). In KS, 62.50% was classifies as low (≤ 2.0 mm/hr), 25% as moderate (> 2.0 and ≤ 4.0 mm/hr), and 12.5 % as high (> 4.0 mm/hr) (Fig.8-B (5)). However, in the other locations, K_{sw} varied between moderate and high level.

For capturing the impact of future change, projected yearly data from the WEPP model were analyzed by comparing baseline values from 2019 (blue dot) with those forecasted values from 2038 (red dot) (Fig.8-C). At first glance, a notable decrease in selected parameters was observed for the three studied ecosystems, where the values of 2019 were generally higher than 2038. For instance, the run-off in the case of KS decreased from 276.1 mm in 2019 to 131.4 mm in 2038. Similarly, RF decreased from 197.7 to 61.5 mm in MN, from 151.6 to 73.9 mm in AINF, and from 199.3 to 32.4 mm in AINBF (Fig.8-C (1)). Soil water erosion followed a similar pattern, with a notable decrease observed in KS location from 2.5 kg/m^2 in 2019 (blue dot) to 0.7 kg/m^2 in 2038 (red dot) (Fig.8-C (2)).

4. Discussion

Under ongoing climate change, soil erosion has become a significant threat to the sustainability of the agricultural sector and the achievement of sustainable development goals. Previously, Borrelli et al. (2017) reported that the global potential soil erosion exceeds 35.9 Pg yr^{-1}, which surpassing, for instance, the soil formation rate of 0.18-0.37 Pg yr-1 in agricultural land in the USA (Pimentel, D., & Burgess, M. (2013), or 0.16-0.75 Pg yr-1 (humus horizon) in global agricultural

land (Lisetskii, F. (2019). Thus, measuring, modeling, and predicting soil erosion by water is a vital activity to maintain ecosystem services. In this research, the WEPP model was used to predict soil erosion in the eastern Mediterranean. First, the model was assessed by comparing the observed data from three ecosystems (four locations) with the predicted data. Results revealed that the model was satisfactory in predicting soil erosion and Run-off, with an acceptable range of errors (Fig 2). However, the WEPP model tends to underestimate run-off in some locations. This could be attributed to the limitation of certain data (rill erodibility, interrill erodibility). Previously, Wang et al. (2023) reported that the WEPP model tends to underestimate run-off for large events, emphasizing the importance of the input baseline data in WEPP calibration. Albaradeyia et al. (2011) reported an underestimation of the WEPP model for both soil erosion and Run-off. The model produced less run-off events compared to the observed data. Similarly, Mohammed et al. (2021) indicated that the WEPP model is unable to accurately predict run-off for large events. Nonetheless, the WEPP model remains within an acceptable range and can be successfully used for forecasting erosion events (Fig 2).

Erosion processes are typically influenced by ecosystem factors, such as soil properties, land cover/land use, and topography (Prashanth et al. 2023; Golkarian et al. 2023). Each element plays a unique role in either accelerating or hindering the erosion process. This research was conducted at four different locations representing three main ecosystems in the eastern Mediterranean. In respective locations, the soil texture ranged from loamy to clayey, with the clay content ranging between 38.12% and 56% (Table 1). High clay content directly impacts the erosion process, particularly in terms of hydraulic conductivity and the initiation of run-off events. This, in turn, affected the accuracy of the model's performance. In this context, Elliot & Flanagan (2023) confirmed that clay content affected the erosion results predicted by the WEPP model influencing the model's erodibility predictions. On the other hand, soil physical characteristics, mainly clay content and organic matter, play a vital role in controlling the soil infiltration process. In the Mediterranean region, soil permeability is high in summer and low in winter due to wetting and swelling processes (Fig. 6-d). In this context, Grønsten and Lundekvam (2006) confirmed that erodibility functions in the WEPP model depend on clay content rather than organic matter content. In the Mediterranean region, physical diagnostic features of clayey soil, such as cracking during the dry season, dynamically influence the erosion process, resulting in preferential flow. This

results in significant differences between the observed run-off and predicted one by WEPP (Raclot & Albergel, 2006).

Land cover plays a crucial role in mitigating soil erosion and delaying run-off (Zhang et al. 2022). Plant leaves absorb the kinetic energy of falling raindrops, indirectly helping to preserve soil aggregates (Ma et al. 202). In the absence of this cover, these aggregates would collapse due to the direct impacts of the kinetic energy of raindrops. Based on the output of this research, the highest erosion and run-off were observed in the agricultural lands, followed by the forest system (Fig. 3, 5, 6, 8). Interestingly, Rostami et al. (2022), observed that soil erosion in crop lands 30-times higher than the forest land. Within the WEPP model, the land cover is represented by the management file. The output of the WEPP model aligns with Rostami et al. (2022), and other studies related to the role of land cover (Fig. 3, 5, 6, 8). Based on the forecasted data, the highest erosion value was recorded in the KS location (Fig. 3, 6, 8), where winter wheat with conventional tillage was the management file. Based on the field survey, the KS location was tilled and planted with pomegranate trees (3-5 years old). Pomegranate is a deciduous tree that leaves the soil bare during the rainy season. For the MN location, winter wheat was the land use, and the WEPP model management file was "Winter Wheat-no till". For both locations, the soil was tilled, and then wheat was planted between September and November. Consequently, the soil is bare, along with the start of the rainy season. Thus, most of the soil erosion and run-off occurred between September and December due to the intensity of rainy storms and bare soil (Fig. 3, 6,). Less erosion was detected in forests and burned forests because the canopy cover protects the upper layer of soil from the direct impact of raindrops.

Future projected results of soil erosion and run-off align with baseline findings, indicating that the highest erosion occurred in the agricultural ecosystem, while the lowest was observed in the forest (Fig 8 c). Overall, in the studied ecosystems, a decreasing trend of both RF and SE was observed comparing with the baseline (Fig 5 e, f). In detail, the projected average annual RF can be ranked as follows: KS (234.7mm ± 75.6) > MN (141.1mm ± 50.2) > AINF (145.4mm ± 47.4) > AINBF (100.3mm ± 49.2). Similarly, SE can be classified as follows: KS (2.38 kg/m² ± 1.36) > AINF (0.45 kg/m² ± 0.17) > MN (0.31 kg/m² ± 0.11) > AINBF (0.24 kg/m² ± 0.15) (Fig. 5, 6). However, the output reveals that the year 2025 is the peak for run-off and erosion events. Tracking various soil parameters and their dynamic response to the erosion process could explain the variation in ecosystem response (Fig. 6).

In all locations, a pattern was observed indicating that erosion could occur between September and May (Fig. 6). Hence, the lowest θ, and highest K_{sw} were recorded in summer. In this context, the KS location exhibited the highest fluctuation, particularly for K_{sw}, with the peak occurring in the summer season. This variation accelerated the soil erosion process. The dry clayey soil at the end of summer and the beginning of the rainy season led to high K_{sw} which decreased gradually to reach minimum values in the winter season as the majority of soil pores were occupied by water (Fig. 6). However, by comparing Fig. 6-a with Fig. 6-c & d results reveal that the intensity of Run-off increased with decreasing K_{sw} and increasing θ values. Interestingly, the forest ecosystem showed an increase in θ values during winter (Fig. 6, green line), which was the highest compared to other systems, while less variation in K_{sw} was observed. This result can be explained by the physicochemical properties of the soil. Forest soil is enriched with organic matter that can absorb water and enhance soil structure (Fig. 6).

5. Limitations and future implementation

In this research, the future projection of climatic variables was produced using the integrated climate generator program, CLIGEN (version 4.3), within the WEPP model. CLIGEN is a weather generator tool utilized by the WEPP model to produce 10 climatic variables for a single location. In this study, CLIGEN was run to generate estimates for a 20-year period (2020–2040).

Previously, CLIGEN has been reported to accurately reproduce rainfall components, such as daily, monthly, and annual totals, as well as extremes, within acceptable error margins. However, it has shown limitations in modeling the duration of storms (Zhang & Garbrecht, 2003). Similarly, Kinnell and Yu (2020) noted that CLIGEN may not consistently provide evenly distributed stochastic rainfall data over extended decades. It is worth noting that CLIGEN has been successfully used in previous studies to simulate various weather scenarios over long periods (e.g., 100 years) to evaluate its impact on both erosion and run-off (Pruski & Nearing, 2002a,b).

For future studies, CMIP5/6 climate data for different time intervals (2020–2040, 2040–2060) could be used to run the model and evaluate ecosystem responses to changes in soil erosion and Run-off. Considering that the quality of daily weather data significantly impacts the model outputs (Zhang & Garbrecht, 2003), future work will involve comparing the outputs of the CLIGEN model with those of CMIP5/6 data. This comparison will help evaluate the agreement and differences

between the datasets, as well as analyze the dynamic response of the WEPP model to these different inputs and their subsequent effects on soil erosion and Run-off.

6. Conclusion remarks

After the current war, an extensive effort is needed to support the sustainability of natural resources in the eastern Mediterranean, especially in the coastal region of Syria. In this research, the WEPP model was used to predict soil erosion and run-off in three Mediterranean ecosystems. The output of this research can be summarized as follow:

- The WEPP model performed well in predicting both soil erosion and Run-off. NSE results revealed a good performance, with almost the same values for RF and ER reaching 0.66 and 0.67, respectively.
- The correlation coefficient (r) reached 0.94 ($p<0.05$) between RF and rainfall, r=0.81 ($p<0.05$) ER vs. rainfall, and r=0.88 ER VS SE. These high correlations between different outputs indicate significant, and robust model output.
- Projected rainfall data using the CLIGEN- WEPP indicated that total annual forecasted rainfall ranged from 800 to 1200 mm. However, the output of the Tukey test revealed that there were no significant differences in the mean yearly rainfall between the historical data (2010-2019) and forecasted one (2020-2040).
- The forecasted run-off varied among locations. The locations can be ranked as: KS (234.7mm±75.6)> MN (141.1mm±50.2)> AINF (145.4mm±47.4) > AINBF (100.3mm±49.2). While for SE, the locations can be classified as: KS (2.38 kg/m^2 ±1.36)> AINF (0.45 kg/m^2 ±0.17) > MN (0.31 kg/m^2 ±0.11)> AINBF (0.24 kg/m^2 ±0.15).
- Land use played a crucial role in influencing erosion process, where the highest erosion values recorded in agricultural ecosystem. Also, Land use significantly other soil properties such as θ and K_{sw}.
- A notable decrease in selected parameters was observed for the three studied ecosystems, where the values of 2019 were generally higher than 2038.

Overall, agricultural ecosystems demonstrate accelerated erosion and run-off compared with other ecosystems. Thus, sustainable agricultural practices are recommended to mitigate soil erosion. Overall, the WEPP model demonstrates good performance and could be used by decision-makers for soil conservation planning.

Conflict of interest: None.

Acknowledgement: covered for reviewing process.

Funding: covered for reviewing process

Author contribution: S.M.: writing review editing.

References:

Abdelwahab, O. M. M., Ricci, G. F., De Girolamo, A. M., & Gentile, F. (2018). Modelling soil erosion in a Mediterranean watershed: Comparison between SWAT and AnnAGNPS models. *Environmental research*, *166*, 363-376.

Abdo, H. G. (2018). Impacts of war in Syria on vegetation dynamics and erosion risks in Safita area, Tartous, Syria. *Regional environmental change*, *18*(6), 1707-1719.

Abdo, H., & Salloum, J. (2017). Spatial assessment of soil erosion in Alqerdaha basin (Syria). *Modeling Earth Systems and Environment*, *3*, 1-7.

Abdo, H. G. (2022). Evaluating the potential soil erosion rate based on RUSLE model, GIS, and RS in Khawabi river basin, Tartous, Syria. *DYSONA-Applied Science*, 3(1), 24-32.

Al-Ali, Y.A.Z.; Kheder, R. (**2014**). Studying the effect of forest fire on soil erosion and loss of some mineral elements in the forest of ein al-jaouz/tartous. *Biol. Sci. Ser., 36*, 277–290. (In Arabic)

Albaradeyia, I., Hani, A., & Shahrour, I. (2011). WEPP and ANN models for simulating soil loss and Run-off in a semi-arid Mediterranean region. *Environmental monitoring and assessment*, *180*, 537-556.

Bakker, M. M., Govers, G., & Rounsevell, M. D. (2004). The crop productivity–erosion relationship: an analysis based on experimental work. *Catena*, *57*(1), 55-76.

Barakat, A., Rafai, M., Mosaid, H., Islam, M. S., & Saeed, S. (2023). Mapping of water-induced soil erosion using machine learning models: a case study of Oum Er Rbia Basin (Morocco). *Earth Systems and Environment*, *7*(1), 151-170.

Borrelli, D.A. Robinson, L.R. Fleischer, E. Lugato, C. Ballabio, C. Alewell, K. Meusburger, S. Modugno, B. Schütt, V. Ferro, V. Bagarello (2017). An assessment of the global impact of 21st century land use change on soil erosion. Nature communications, 8(1).

Borrelli, P., Robinson, D. A., Fleischer, L. R., Lugato, E., Ballabio, C., Alewell, C., ... & Panagos, P. (2017). An assessment of the global impact of 21st century land use change on soil erosion. *Nature communications*, *8*(1), 1-13.

Chen, J., Zhang, X. C., Liu, W. Z., & Li, Z. (2009). Evaluating and Extending CLIGEN Precipitation Generation for the Loess Plateau of China 1. *JAWRA Journal of the American Water Resources Association*, *45*(2), 378-396.

Comino, J. R., Iserloh, T., Lassu, T., Cerdà, A., Keestra, S. D., Prosdocimi, M., ... & Ries, J. B. (2016). Quantitative comparison of initial soil erosion processes and Run-off generation in Spanish and German vineyards. *Science of the Total Environment*, *565*, 1165-1174.

d'Oleire-Oltmanns, S., Marzolff, I., Peter, K. D., & Ries, J. B. (2012). Unmanned aerial vehicle (UAV) for monitoring soil erosion in Morocco. *Remote sensing*, *4*(11), 3390-3416.

Duan, X., Xie, Y., Ou, T., & Lu, H. (2011). Effects of soil erosion on long-term soil productivity in the black soil region of northeastern China. Catena, 87(2), 268-275.

Elliot, W. J., & Flanagan, D. C. (2023). Estimating WEPP cropland erodibility values from soil properties.

Flanagan, D. C., & Nearing, M. A. (1995). USDA-Water Erosion Prediction Project: Hillslope profile and watershed model documentation. *NSERL report*, *10*, 1196-47097. USDA-ARS National Soil Erosion Research Laboratory, West Lafayette, Indiana 47907.

Flanagan, D. C., Gilley, J. E., & Franti, T. G. (2007). Water Erosion Prediction Project (WEPP): Development history, model capabilities, and future enhancements. *Transactions of the ASABE*, *50*(5), 1603-1612.

García-Ruiz, J. M. (2010). The effects of land uses on soil erosion in Spain: A review. *Catena*, *81*(1), 1-11.

Golkarian, A., Khosravi, K., Panahi, M., & Clague, J. J. (2023). Spatial variability of soil water erosion: Comparing empirical and intelligent techniques. *Geoscience Frontiers*, *14*(1), 101456.

Gómez, J. A., Infante-Amate, J., González de Molina, M., Vanwalleghem, T., Taguas, E. V., & Lorite, I. (2014). Olive cultivation, its impact on soil erosion and its progression into yield impacts in Southern Spain in the past as a key to a future of increasing climate uncertainty. *Agriculture*, *4*(2), 170-198.

Griggs, D, Stafford-Smith M, Gaffney O, Rockström J, Öhman M C, Shyamsundar P, Steffen W, Glaser G, Kanie N, and Noble N. 2013. "Sustainable Development Goals for People and Planet." Nature 495 (7441): 305–7.

Grønsten, H. A., & Lundekvam, H. (2006). Prediction of surface Run-offand soil loss in southeastern Norway using the WEPP Hillslope model. *Soil and Tillage Research*, *85*(1-2), 186-199.

Keesstra, S. D., Bouma, J., Wallinga, J., Tittonell, P., Smith, P., Cerdà, A., Montanarella, L., Quinton, J.N., Pachepsky, Y., van der Putten, W.H., Bardgett, R.D., Moolenaar, S., Mol, G., Jansen, B., & Fresco, L. O. (2016). The significance of soils and soil science towards realization of the United Nations Sustainable Development Goals. Soil, 2(2), 111-128.

Kheir, R. B., Cerdan, O., & Abdallah, C. (2006). Regional soil erosion risk mapping in Lebanon. *Geomorphology*, *82*(3-4), 347-359.

Kinnell, P. I., & Yu, B. (2020). CLIGEN as a weather generator for predicting rainfall erosion using USLE based modelling systems. *Catena*, *194*, 104745.

Kulimushi, L. C., Choudhari, P., Mubalama, L. K., & Banswe, G. T. (2021a). GIS and remote sensing-based assessment of soil erosion risk using RUSLE model in South-Kivu province, eastern, Democratic Republic of Congo. *Geomatics, Natural Hazards and Risk*, *12*(1), 961-987.

Kulimushi, L. C., Maniragaba, A., Choudhari, P., Elbeltagi, A., Uwemeye, J., Rushema, E., & Singh, S. K. (2021b). Evaluation of soil erosion and sediment yield spatio-temporal pattern during 1990–2019. *Geomatics, Natural Hazards and Risk*, *12*(1), 2676-2707.

Lisetskii, F. (2019). Estimates of soil renewal rates: applications for anti-erosion arrangement of the agricultural landscape. *Geosciences*, *9*(6), 266.

Ma, R., Hu, F., Xu, C., Liu, J., & Zhao, S. (2022). Response of soil aggregate stability and splash erosion to different breakdown mechanisms along natural vegetation restoration. *Catena*, *208*, 105775.

Mahmoodabadi, M., & Cerdà, A. (2013). WEPP calibration for improved predictions of interrill erosion in semi-arid to arid environments. *Geoderma*, *204*, 75-83.

Meinen, B. U., & Robinson, D. T. (2021). Agricultural erosion modelling: Evaluating USLE and WEPP field-scale erosion estimates using UAV time-series data. *Environmental Modelling & Software*, *137*, 104962.

Miller, J. E. (1984). *Basic concepts of kinematic-wave models* (No. 1302). US Geological Survey.

Mohammed, S., Alaa, K., Omran, A., Quoc, B. P., Nguyen, T. T. L., Van, N. T., ... & Endre, H. (2021b). Predicting soil erosion hazard in Lattakia Governorate (W Syria). *International Journal of Sediment Research*, *36*(2), 207-220.

Mohammed, S., Alsafadi, K., Talukdar, S., Kiwan, S., Hennawi, S., Alshihabi, O., ... & Harsanyie, E. (2020). Estimation of soil erosion risk in southern part of Syria by using RUSLE integrating geo informatics approach. *Remote Sensing Applications: Society and Environment*, *20*, 100375.

Mohammed, S., Hassan, E., Abdo, H. G., Szabo, S., Mokhtar, A., Alsafadi, K., ... & Rodrigo-Comino, J. (2021a). Impacts of rainstorms on soil erosion and organic matter for different cover crop systems in the western coast agricultural region of Syria. *Soil Use and Management*, *37*(1), 196-213.

Mohammed, S., Hassan, E., Abdo, H. G., Szabo, S., Mokhtar, A., Alsafadi, K., ... & Rodrigo-Comino, J. (2021b). Impacts of rainstorms on soil erosion and organic matter for different cover crop systems in the western coast agricultural region of Syria. *Soil Use and Management*, *37*(1), 196-213.

Mohammed, S., Hussien, M., Alsafadi, K., Mokhtar, A., Rianna, G., Kbibo, I., ... & Harsanyi, E. (2021c). Assessing the WEPP model performance for predicting daily Run-off in three terrestrial ecosystems in western Syria. *Heliyon*, *7*(4).

Mohammed, S., Jouhra, A., Enaruvbe, G. O., Bashir, B., Barakat, M., Alsilibe, F., ... & Szabó, S. (2023). Performance evaluation of machine learning algorithms to assess soil erosion in Mediterranean farmland: A case-study in Syria. *Land Degradation & Development*, *34*(10), 2896-2911.

Mohammed, S., Khallouf, A., Kiwan, S., Alhenawi, S., Ali, H., Harsányi, E., ... & Habib, H. (2020). Characterization of major soil orders in Syria. *Eurasian Soil Science*, *53*, 420-429.

Nearing, M. A. (1998). Why soil erosion models over-predict small soil losses and under-predict large soil losses. *Catena*, *32*(1), 15-22.

Nunes, A. N., Gonçalves, J. P., & Figueiredo, A. (2023). Soil erosion in extensive versus intensive land uses in areas sensitive to desertification: A case study in Beira Baixa, Portugal. *Land*, *12*(8), 1591.

Pampalone, V., Carollo, F. G., Nicosia, A., Palmeri, V., Di Stefano, C., Bagarello, V., & Ferro, V. (2022). Measurement of Water Soil Erosion at Sparacia Experimental Area (Southern Italy): A Summary of More than Twenty Years of Scientific Activity. *Water*, *14*(12), 1881.

Pimentel, D., & Burgess, M. (2013). Soil erosion threatens food production. *Agriculture*, *3*(3), 443-463.

Poesen, J. (2018). Soil erosion in the Anthropocene: Research needs. Earth Surface Processes and Landforms, 43(1), 64-84. https://doi.org/10.1002/esp.4250

Prashanth, M., Kumar, A., Dhar, S., Verma, O., Rai, S. K., & Kouser, B. (2023). Land use/land cover change and its implication on soil erosion in an ecologically sensitive Himachal Himalayan watershed, Northern India. *Frontiers in Forests and Global Change*, *6*, 1124677.

Pruski, F. F., & Nearing, M. A. (2002a). Run-offand soil-loss responses to changes in precipitation: A computer simulation study. *Journal of soil and Water Conservation*, *57*(1), 7-16.

Pruski, F. F., & Nearing, M. A. (2002b). Climate-induced changes in erosion during the 21st century for eight US locations. *Water Resources Research*, *38*(12), 34-1.

Raclot, D., & Albergel, J. (2006). Run-offand water erosion modelling using WEPP on a Mediterranean cultivated catchment. *Physics and Chemistry of the Earth, Parts A/B/C*, *31*(17), 1038-1047.

Raclot, D., & Albergel, J. (2006). Run-offand water erosion modelling using WEPP on a Mediterranean cultivated catchment. *Physics and Chemistry of the Earth, Parts A/B/C*, *31*(17), 1038-1047

Renard, K. G. (1997). *Predicting soil erosion by water: a guide to conservation planning with the Revised Universal Soil Loss Equation (RUSLE)*. US Department of Agriculture, Agricultural Research Service.

Rostami, N., Heydari, M., Uddin, S. M., Esteban Lucas-Borja, M., & Zema, D. A. (2022). Hydrological response of burned soils in croplands, and pine and oak forests in Zagros forest ecosystem (western Iran) under rainfall simulations at micro-plot scale. *Forests*, *13*(2), 246.

Richi, S. M. (2025). Integrated RUSLE-GIS modeling for enhancing soil erosion management in Ghamima River Basin, Syria. *DYSONA-Applied Science*, *6*(1), 104-112.

Saghafian, B., Meghdadi, A. R., & Sima, S. (2015). Application of the WEPP model to determine sources of run-off and sediment in a forested watershed. *Hydrological Processes*, *29*(4), 481-497.

Sahour, H., Gholami, V., Vazifedan, M., & Saeedi, S. (2021). Machine learning applications for water-induced soil erosion modeling and mapping. *Soil and Tillage Research*, *211*, 105032.

Shen, Z. Y., Gong, Y. W., Li, Y. H., Hong, Q., Xu, L., & Liu, R. M. (2009). A comparison of WEPP and SWAT for modeling soil erosion of the Zhangjiachong Watershed in the Three Gorges Reservoir Area. *Agricultural Water Management*, *96*(10), 1435-1442.

Soto, B., & Díaz-Fierros, F. (1998). Run-offand soil erosion from areas of burnt scrub: comparison of experimental results with those predicted by the WEPP model. *Catena*, *31*(4), 257-270.

Tenge, A. J., Kaihura, F. B. S., Lal, R., & Singh, B. R. (1998). Erosion effects on soil moisture and corn yield on two soils at Mlingano, Tanzania. *American journal of alternative agriculture*, *13*(2), 83-89.

van Leeuwen, C. C., Cammeraat, E. L., de Vente, J., & Boix-Fayos, C. (2019). The evolution of soil conservation policies targeting land abandonment and soil erosion in Spain: A review. *Land use policy*, *83*, 174-186.

Varvani, J., Khaleghi, M. R., & Gholami, V. (2019). Investigation of the relationship between sediment graph and hydrograph of flood events (case study: Gharachay River Tributaries, Arak, Iran). Water Resources, 46(6), https://doi.org/883-893

Wang, S., McGehee, R. P., Guo, T., Flanagan, D. C., & Engel, B. A. (2023). Calibration, validation, and evaluation of the Water Erosion Prediction Project (WEPP) model for hillslopes with natural Run-offplot data. *International Soil and Water Conservation Research*, *11*(4), 669-687.

Wang, S., McGehee, R. P., Guo, T., Flanagan, D. C., & Engel, B. A. (2023). Calibration, validation, and evaluation of the Water Erosion Prediction Project (WEPP) model for hillslopes with natural Run-offplot data. *International Soil and Water Conservation Research*, *11*(4), 669-687.

Zachar, D. *Soil Erosion*; Cowan, M., Ed.; Elsevier Scientific Pub. Co.: New York, NY, USA, 1982.

Zhang, X., Song, J., Wang, Y., Sun, H., & Li, Q. (2022). Threshold effects of vegetation coverage on Run-offand soil loss in the Loess Plateau of China: A meta-analysis. *Geoderma*, *412*, 115720.

Zhang, X. C., & Garbrecht, J. D. (2003). Evaluation of CLIGEN precipitation parameters and their implication on WEPP Run-offand erosion prediction. *Transactions of the ASAE*, *46*(2), 311.

Zhu, R., Yu, Y., Zhao, J., Liu, D., Cai, S., Feng, J., & Rodrigo-Comino, J. (2023). Evaluating the applicability of the water erosion prediction project (WEPP) model to Run-offand soil loss of sandstone reliefs in the Loess Plateau, China. *International Soil and Water Conservation Research*, *11*(2), 240-250.

Declaration of interests

☒ The authors declare that they have no known competing financial interests or personal relationships that could have appeared to influence the work reported in this paper.

☐The authors declare the following financial interests/personal relationships which may be considered as potential competing interests: